MORPHOLOGICAL ANALYSIS OF THE PAPILLARY MUSCLES AND THE TRABECULAE

Mingchen Gao[1], *Chao Chen*[1], *Shaoting Zhang*[2], *Zhen Qian*[3], *Mani Vannan*[3], *Sarah Rinehart*[3], *Dimitris Metaxas*[1], *Leon Axel*[4]

[1]CBIM, Rutgers University, Piscataway, NJ
[2]Department of Computer Science, UNC Charlotte, Charlotte, NC
[3]Piedmont Heart Institute, Atlanta, GA [4]New York University, 660 First Avenue, New York, NY

ABSTRACT

High resolution cardiac CT imaging technology has revealed the complex endocardial structures of the left ventricle, such as the trabeculae and the papillary muscles. In this paper, we study the morphology of such complex structures. We represent the structures accurately and concisely using curve skeletons, and measure these structures using topological and geometrical features. It is observed both qualitatively and quantitatively that structures at different parts of the endocardial surface have different characteristics. This morphological study sheds light on the potential future use of these complex endocardial structures to study cardiac function and to diagnose cardiac diseases.

1. INTRODUCTION

Heart disease is the deadliest disease worldwide. Detecting/diagnosing such diseases in their early stages is critical, and heavily depends on non-invasive imaging methods, e.g., computed tomography (CT) and magnetic resonance imaging (MRI). Images acquired using these technologies are fed into image segmentation algorithms to extract anatomical structures such as left ventricle (LV) and right ventricle (RV) [12]. Based on the segmentation results, various parameters are extracted and used for analyzing cardiac function and diagnosing cardiac diseases. There are global features such as ejection fraction (EF), ventricular volume and myocardial mass [14]. In order to detect local abnormalities, e.g., related to LV hypertrophy (LVH) or severe aortic stenosis (AS), regional features such as myocardial strain [16], wall thickness [1] and local contraction of the endocardial surface [13] have also been studied.

Although many measurements have been developed, it is surprising that we still cannot characterize the detailed endocardial surface structures that have been documented since 1513 [17], namely, the *trabeculae* and the *papillary muscles* (TPM). Some trabeculae are completely attached to the wall of the heart, while others are fixed at both ends to the ventricular wall, but the intermediate section is freely mobile within the cavity, forming topological handles. The papillary muscles are attached to the valves via chordae tendineae. They start contracting shortly before the ventricle contraction starts, so valves function properly during a cardiac cycle. See illustrations in Fig. 1.

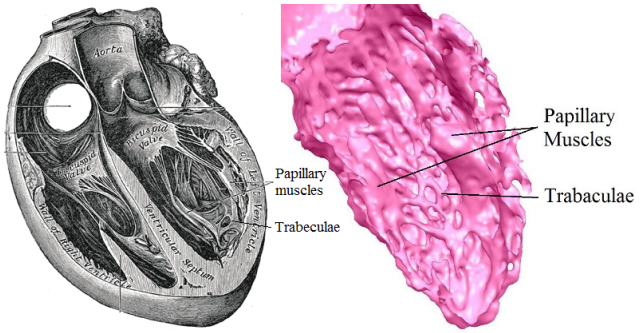

Fig. 1. Left: Heart anatomy (from [8]). Right: Segmentation of LV capturing the papillary muscles and the trabeculae.

The study of these complex structures is very important. A recent study shows that TPM structures composes up to 23% of LV end-diastolic volume in average [3]. Therefore, an accurate measurement of TPM is critical for any study using volume-related metrics. Furthermore, an accurate extraction of TPM is the prerequisite for an accurate simulation of blood flow in ventricles [9]. In terms of clinical impact, there are hypotheses about correlations between TPM and cardiac diseases like LVH, AS, thrombus and stroke [15]. The investigation of TPM was underdeveloped due to the limitation of traditional imaging modality. The new technology of high resolution CT enables us to capture the fine TPM structures in a higher accuracy. Using new segmentation methods inspired from computational topology, Gao *et al*. [6, 7] accurately reconstructed the fine and complex structure from these high resolution CT images. The acquired TPM structures are used for further analysis. Zhong *et al*. [18] extracted and quantitatively characterized the motion of papillary muscles. Differences between healthy and hypertrophic papillary muscles were observed. Mukhopadhyay *et al*. [11] studied the LV endocardial surface using an isometry-invariant bag-of-words (BOW) feature. They chose descriptors invariant to isometric

deformations and achieved effective incidence of coronary arterial stenosis localization. However, the BOW method, as a black box characterization of the endocardial surface, cannot give clinically insightful explanation of the diseased regions or provide specifically effective features.

In this paper, we study the morphology of the trabeculae and the papillary muscles. We design a framework to segment TPM and then extract their skeleton, giving us convenient tools for measurement and visualization. A set of features are proposed and computed, which characterize the structures in terms of both topology and geometry. Our analysis reveals that these TPM have different characteristics in different locations. We believe our preliminary study can be used clinically in the future.

2. METHODOLOGY

Our system first accurately segments the structures from high resolution CT images, then extracts skeletons of trabeculae. Finally we compute features based on these skeletons.

2.1. Topologically Accurate Segmentation

In order to analyze the papillary muscles and the trabeculae, a high quality segmentation which captures these fine structures is required. Gao *et al*. [6] proposed a method to segment 3D high resolution CT data by explicitly restoring topological handles, which happen regularly in the detailed structures. The location and geometry of these handles are suggested by a tool from computational topology, namely, persistent homology [5]. Intuitively speaking, a suggested handle should have high saliency, which is defined as the difference between the maximal intensity value along the handle and the maximal value of the best 3D patch sealing the handle up. The method has been proved to be accurate both topologically and geometrically. Fig. 3 (left) shows a representative segmentation result.

2.2. Skeleton Extraction

Since trabeculae have the shape of tubes, it is natural to represent them using skeletons, namely, pieces of 1-manifolds with boundaries stitched together at vertices. See Figure 3 for an illustration. Computed skeletons will be used for our visualization and morphological analysis.

We choose the *curve skeleton* defined by Dey and Sun [4] because of its numerical stability and robustness. A curve skeleton is a subset of the medial axis of a given 3D object, which includes the trabeculae and the papillary muscles in our case. The *medial axis* is the set of points each of which is the center of a ball, B_x, contained in the 3D object and that touches the surface in at least 2 points. The *medial geodesic function* of a point x in the medial axis is the shortest geodesic distance between the two touching points of B_x within the surface. The curve skeleton is then defined as the singularities, namely, non-differentiable points of this medial geodesic function. One may also use the radius of the ball B_x, instead, for the definition. The difference between the two definitions is marginal when the trabeculae are close to tubes.

2.3. Features

We design and compute several features to describe the morphology of the trabeculae and the papillary muscles. The extracted trabeculae (Fig. 3 (left) and Fig. 4) are generally in the form of triangular meshes. In order to describe the complexity of such structures, we would like to count the number of handles and tunnels. This can be calculated using a metric from algebraic topology, i.e., the *Betti number*. Beside topological complexity, we also would like to measure the geometry, like how wiggly and how thick these handles are. Therefore we use geometric features like *length* and *diameter*. Next, we define these features in details.

One-dimensional Betti number: The *genus* of an orientable surface is the maximum number of cutting planes that could be applied before cutting the surface into disconnected components. Intuitively, the genus counts the number of handles of a surface. We could approximately compute the genus of a surface as a half of the one-dimensional *Betti number*, β_1 (Fig.2 left). To compute the Betti number, we extract from a mesh of the endocardial surface two boundary matrices, ∂_1 and ∂_2. The former, ∂_1, is the adjacency matrix of the graph, which consists of all vertices and edges of the mesh. The latter, ∂_2, is similarly defined, except that each row corresponds to an edge and each column corresponds to a triangle of the mesh. The one-dimensional Betti number is then computed as $\beta_1 = rank(kernel(\partial_1)) - rank(\partial_2)$, where $rank$ is the rank of a vector space and $kernel$ is the nullspace of a linear operator [5].

Length: While the one-dimensional Betti number describes the topological complexity of the structure, the *total length* of a trabecula is used to describe its geometrical complexity. It is measured by calculating the total length of the extracted skeleton.

Diameter: The *diameter* at a particular point of the trabecula is the diameter of the intersection disk of the trabecula and a cutting plane. The cutting plane is selected to be perpendicular to the tangent of the skeleton (Fig. 2 right).

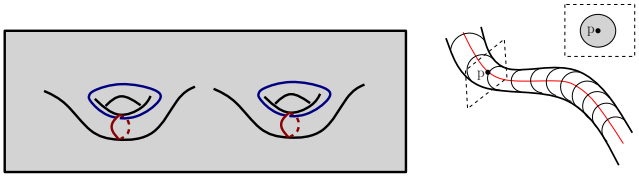

Fig. 2. Left: a surface with genus two (two handles). The Betti number is four. Right: the diameter at point p is measured by the perimeter of the intersection disk.

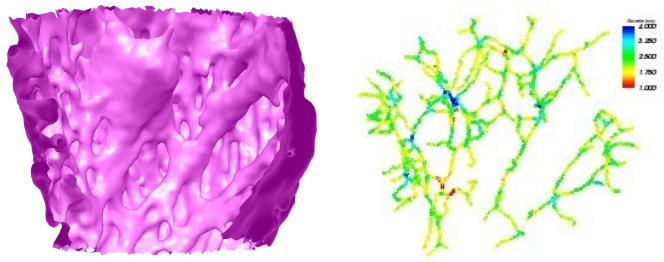

Fig. 3. Left: Endocardial surface. Right: Curve skeleton colored by diameter.

3. EXPERIMENTS AND DISCUSSION

We employed the proposed method to analyze 10 healthy human cardiac multidetector CT (MDCT) data sets. The CT data were acquired on a 320-MDCT scanner, using a conventional ECG-gated contrast-enhanced CT angiography protocol with the following parameters: prospectively triggered, single-beat, volumetric acquisition; tube voltage 120 kV, tube current $200 - 550$ mA. The detector width was 0.5mm. The CT images were reconstructed at 75% in the R-R cardiac cycle to ensure minimal ventricular motion. The spatial resolution varied from 0.3 mm to 0.5 mm. The matrix size of reconstructed images was 512 by 512 by 320.

3.1. Skeleton Extraction Validation

We started our experiments by validating the accuracy of the skeleton extraction. We compared our curve skeleton result to the skeleton computed using the classical morphological operators [10], *thinning*. Fig. 3 shows the left endocardial surface mesh and the curve skeleton extracted from it. To quantitatively evaluate the accuracy of the skeleton extracted, we computed the distance from curve skeleton to thinning and the reverse. The average distances between curve skeleton to thinning skeleton and reverse are 0.52 ± 0.42 voxels and 1.02 ± 1.39 voxels, respectively. In summary, the curve skeleton gives a good approximation of the true skeleton and can be used for visualization and measuring of trabeculae.

3.2. Morphological Analysis

The segmentation and skeleton extraction algorithms were firstly applied to get a triangle mesh and a skeleton abstraction. We observed the spatial distribution of the trabeculae varies with the location within the LV. Consistent with the standard anatomical description [8], we observed three types of trabeculae (Fig.4).

1. Attached to the wall along their entire length and formed as prominent ridges of the heart wall. Located approximately in the left circumflex coronary artery area. These trabeculae are generally thick and have a consistent orientation and diameter.
2. Fixed at their extremities but free in the middle. Located approximately near the two papillary muscles. They have small diameter and inconsistent orientation.
3. Located on the apices of the papillary muscles, which give origin to the chordae tendineae.

We further divided the mesh into 17 segments according to the AHA model [2] to perform regional shape analysis (Fig. 5). Different segments clearly have different trabeculae complexity. This observation is verified quantitatively using the proposed features.

We measured the proposed features on 10 data sets, each of which had been reconstructed and further divided into segments. Fig. 5 left shows regional properties of different segments of the LV. We also illustrate the pattern of proposed features in different regions, using a bull's eye visualization (Fig. 6). While the Betti number and length features illustrate apparent differences between different regions, it is difficult to distinguish regions using diameter alone.

We performed statistical analysis to measure the significance of the differences in features between different regions, using t-test. We found that the difference between different regions was indeed statistically significant. The p-value of differences between one-dimensional Betti number and total lengths of segment 8 (mid anteroseptal) and segment 11 (mid inferolateral) are 4.8×10^{-4} and 1.6×10^{-3}, respectively. Taking segment 4, using total length feature for example, segments $1, 5, 6, 7, 10, 11, 12, 13, 14, 16$ did not reject the null hypothesis, which means those regions are not independent. For segment 8 using one-dimensional Betti number feature, segments $2, 3, 9$ did not reject the null hypothesis. Thus, as expected, the septum has quantifiable differences in trabeculation from the free wall.

4. CONCLUSION

In this paper, we proposed a method to analyze the complex endocardial structures, namely, the papillary muscles and the trabeculae. There are several directions for the future work. Closely looking at the quantitative features of normal hearts and diseased hearts would also provide insight, once diseased

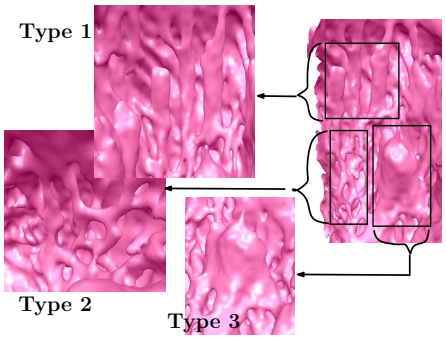

Fig. 4. Three types of trabeculae.

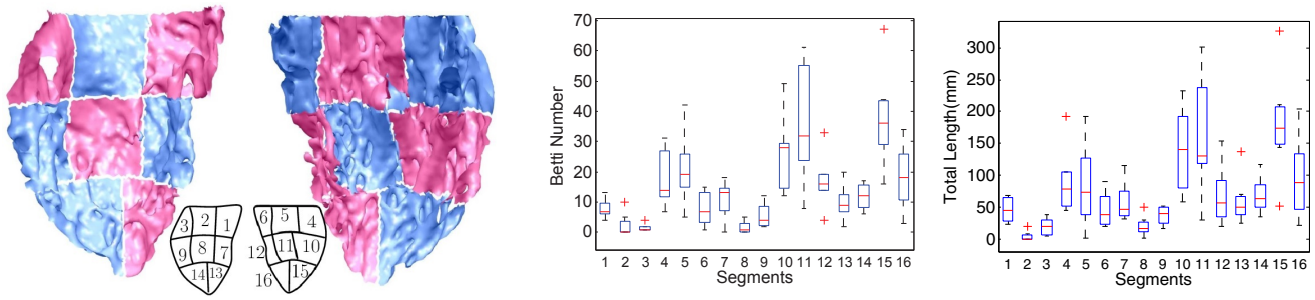

Fig. 5. From left to right: 17 Segments of the LV. One-dimensional Betti number, total length of LV segments. Red line is the median of data, blue box shows the range of 25% to 75% of the data. Black dots represents the range.

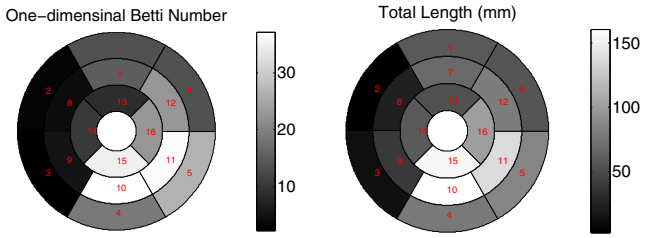

Fig. 6. Bull's eye visualization of the mean values of Betti number and length features on 17 segments.

samples are available. This work can also be extended to a full spatio-temporal cardiac image analysis.

Acknowledgement: This work is supported by NIH-R21HL88354-01A1, Multiscale Quantification of 3D LV Geometry from CT.

References

[1] E. Castillo, J. A. Lima, and D. A. Bluemke. Regional myocardial function: Advances in MR imaging and analysis1. *Radiographics*, 23(suppl 1):S127–S140, 2003.

[2] M. D. Cerqueira, N. J. Weissman, V. Dilsizian, A. K. Jacobs, S. Kaul, W. K. Laskey, D. J. Pennell, J. A. Rumberger, T. Ryan, M. S. Verani, et al. Standardized myocardial segmentation and nomenclature for tomographic imaging of the heart a statement for healthcare professionals from the cardiac imaging committee of the Council on Clinical Cardiology of the American Heart Association. *Circulation*, 105(4):539–542, 2002.

[3] M. L. Chuang, P. Gona, G. L. Hautvast, C. J. Salton, S. J. Blease, S. B. Yeon, M. Breeuwer, C. J. O'Donnell, and W. J. Manning. Correlation of trabeculae and papillary muscles with clinical and cardiac characteristics and impact on CMR measures of LV anatomy and function. *JACC: Cardiovascular Imaging*, 5(11):1115–1123, 2012.

[4] T. K. Dey and J. Sun. Defining and computing curve-skeletons with medial geodesic function. In *Symposium on Geometry Processing*, pages 143–152, 2006.

[5] H. Edelsbrunner and J. Harer. *Computational topology: an introduction*. Amer Mathematical Society, 2010.

[6] M. Gao, C. Chen, S. Zhang, Z. Qian, D. Metaxas, and L. Axel. Segmenting the papillary muscles and the trabeculae from high resolution cardiac CT through restoration of topological handles. In *IPMI*, volume 7917, pages 184–195. 2013.

[7] M. Gao, J. Huang, S. Zhang, Z. Qian, S. Voros, D. N. Metaxas, and L. Axel. 4D cardiac reconstruction using high resolution CT images. In *FIMH*, pages 153–160, 2011.

[8] H. Gray. *Anatomy of the human body*. Lea & Febiger, 1918.

[9] S. Kulp, M. Gao, S. Zhang, Z. Qian, S. Voros, D. Metaxas, and L. Axel. Using high resolution cardiac CT data to model and visualize patient-specific interactions between trabeculae and blood flow. In *MICCAI 2011*, pages 468–475. Springer, 2011.

[10] T.-C. Lee, R. L. Kashyap, and C.-N. Chu. Building skeleton models via 3-D medial surface/axis thinning algorithms. *CVGIP: Graph. Models Image Process.*, 56(6):462–478, Nov. 1994.

[11] A. Mukhopadhyay, Z. Qian, S. M. Bhandarkar, T. Liu, S. Rinehart, and S. Voros. Morphological analysis of the left ventricular endocardial surface and its clinical implications. In *MICCAI 2012*, pages 502–510. Springer, 2012.

[12] C. Petitjean and J.-N. Dacher. A review of segmentation methods in short axis cardiac MR images. *Medical Image Analysis*, 15(2):169–184, 2011.

[13] A. Pourmorteza, K. H. Schuleri, D. A. Herzka, A. C. Lardo, and E. R. McVeigh. A new method for cardiac computed tomography regional function assessment stretch quantifier for endocardial engraved zones (squeez). *Circulation: Cardiovascular Imaging*, 5(2):243–250, 2012.

[14] T. Schlosser, K. Pagonidis, C. U. Herborn, P. Hunold, K.-U. Waltering, T. C. Lauenstein, and J. Barkhausen. Assessment of left ventricular parameters using 16-MDCT and new software for endocardial and epicardial border delineation. *American Journal of Roentgenology*, 184(3):765–773, 2005.

[15] J. T. Vermeulen, M. A. Mcguire, T. Opthof, R. Coronel, J. M. De Bakker, C. Klöpping, and M. J. Janse. Triggered activity and automaticity in ventricular trabeculae of failing human and rabbit hearts. *Cardiovascular research*, 28(10):1547–1554, 1994.

[16] H. Wang and A. A. Amini. Cardiac motion and deformation recovery from MRI: A review. *TMI*, 31(2):487–503, 2012.

[17] F. Wells. Leonardos heart. In *The Heart of Leonardo*, pages 173–242. Springer London, 2013.

[18] L. Zhong, S. Zhang, M. Gao, J. Huang, Z. Qian, D. Metaxas, and L. Axel. Papillary muscles analysis from high resolution CT using spatial-temporal skeleton extraction. In *ISBI*, 2013.